Draft version May 11, 2020
Preprint typeset using LaTeX style emulateapj v. 08/13/06

# NEARBY QUINTUPLE SYSTEMS $\kappa$ TUCANAE AND $\xi$ SCORPII

Andrei Tokovinin
Cerro Tololo Inter-American Observatory,* Casilla 603, La Serena, Chile
*Draft version May 11, 2020*

## ABSTRACT

Architecture and parameters of two wide nearby hierarchical systems containing five solar-type stars each, $\kappa$ Tuc and $\xi$ Sco, are studied. Using *Gaia* astrometry and photometry, masses are determined from visual orbits and isochrones, effective temperatures from spectra or colors. Both systems are $\sim$2 Gyr old. Their spatial motion corresponds to young disk but does not match any known kinematic group. Internal proper motions relative to the center of mass and radial velocities show that wide $\sim$ 8 kau outer pairs are bound. No correlation between orbit orientations in the inner subsystems is observed. All masses except one are confined to the narrow range from 0.8 to 1.5 solar. Strongly correlated masses and wide orbits can be explained if those systems formed by fragmentation in relative isolation and their components accreted gas from common source, as expected in a hierarchical collapse. Young moving groups could be formed in similar environments, and many of them contain high-order hierarchies.

*Subject headings:*

## 1. INTRODUCTION

Stellar hierarchical systems with five or six components occupy intermediate position between single and binary stars on one hand and moving groups and clusters on the other. Their architecture can throw light on the formation of these systems and therefore complement the general picture of star formation. New observations, in particular precise astrometry from *Gaia* (Gaia collaboration 2018), allow study of relative motions with unprecedented accuracy. Meanwhile, recent hydrodynamical simulations of star formation (Bate 2019; Lee et al. 2019; Kuffmeier et al. 2019) provide details of complex mechanisms involved in the genesis of stellar hierarchies.

High-order hierarchies are rare, but by no means exceptional. Even the nearest star, $\alpha$ Cen, is a triple system. According to Duchêne & Kraus (2013), the fraction of systems with $N$ components drops as $3.7^{-N}$. The fraction of triples among solar-type stars is 0.13 (Tokovinin 2014), so 1% of all systems can be quintuple, and such hierarchies are found even in the small sample within 25 pc (Raghavan et al. 2010). The nearest quintuple systems are GJ 644 (J16555−08200) at 6.4 pc and $\xi$ UMa (J11182+3122) at 8.3 pc. The two quintuples studied here, $\kappa$ Tuc and $\xi$ Sco, are located at 21 and 28 pc, respectively, and are composed of solar-type stars.

The Multiple Star Catalog, MSC (Tokovinin 2018), counts 82 entries with five or more components. Architecture of these systems is quite diverse. Some are very young and contain pre-main sequence (PMS) components. Many are members of young moving groups (YMGs), for example $\alpha$ Gem (Castor), $\beta$ Tuc, $\epsilon$ Cha, and $\zeta$ UMa. Caballero (2010) discussed an ultra-wide (1 pc separation) multiple system $\alpha$ Lib and AU Lib belonging to the Castor group and noted a relation between YMGs and hierarchies. He argued that this system is gravitationally bound and not just a pair of group members. However, the borderline between YMGs and very wide stellar systems remains fuzzy.

High-order stellar hierarchies often contain one or more close spectroscopic subsystems. For example, there are three spectroscopic pairs in Castor. However, the two quintuples studied here do not contain close subsystems and their wide pairs fit within the canonical upper limit of 10 kau. Moreover, these hierarchies have an age of $\sim$2 Gyr and, therefore, do not belong to YMGs. The goal of this study is to investigate motions and composition of these interesting systems and to propose a scenario of their formation.

Basic information on the architecture of the two selected quintuples and parameters of their components are given in Section 2, then each system is discussed in detail in Sections 3 and 4. Common data and methods are also presented in Section 2. Formation of these hierarchies is discussed in Section 5.

## 2. OBJECTS, DATA, AND METHODS

Details on each individual system are given in the two following Sections. Here, basic information on both systems is assembled, common data sources and methods are presented.

### 2.1. *Structure and parameters of $\kappa$ Tuc and $\xi$ Sco*

I study here two bright nearby quintuple system composed of solar-type stars, $\kappa$ Tuc and $\xi$ Sco. These stars have extensive literature and a good observational history. Nevertheless, only $\xi$ Sco has been analyzed so far as a quintuple system (van de Kamp & Harrington 1964; Anosova & Orlov 1991). Figure 1 shows the architecture of these systems. Components (individual stars and centers of mass) are denoted by one or several letters, systems are designated by joining their components with comma. For example, A,B refers to the subsystem containing stars A and B, while AB stands for the center of mass of this pair in a wider subsystem AB,C.

Table 1 lists data on the components. The adopted parallax of each system and the proper motion (PM)

*NSF's National Optical-Infrared Astronomical Research Laboratory
Electronic address: atokovinin@ctio.noao.edu

TABLE 1
DATA ON COMPONENTS OF $\kappa$ TUC AND $\xi$ SCO

| Comp | HD | $V$ mag | $G$ mag | Sp. type | $T_e$ K | Mass $M_\odot$ | $\varpi$ mas | $\mu^*_\alpha$ mas yr$^{-1}$ | $\mu_\delta$ mas yr$^{-1}$ | RV km s$^{-1}$ |
|---|---|---|---|---|---|---|---|---|---|---|
| | $\kappa$ Tuc | 01158−6853 | | | | | **47.66** | **392.7** | **106.2** | |
| A | 7788 | 4.88 | 4.79 | F6IV | 6513 | 1.35 | 47.653 | 409.2 | 107.0 | 8.0 |
| B | ... | 7.54 | 7.32 | G5V | 5145 | 0.88 | 47.528 | 386.3 | 82.4 | 8.2 |
| C | 7693 | 7.76 | 7.45 | K2V | 5062 | 0.86 | 47.662 | 360.5 | 95.4 | 5.6 |
| D | ... | 8.26 | 7.94 | K3V | 4850 | 0.80 | 47.800 | 426.2 | 121.3 | ... |
| | $\xi$ Sco | 16044−1122 | | | | | **35.84** | **−61.3** | **−22.2** | |
| A | 144070 | 4.84 | 4.772 | ... | 6532 | 1.53 | 35.31: | −74.3 | −32.9 | ... |
| B | 144069 | 4.86 | 4.767 | ... | 6532 | 1.53 | 36.24: | −41.9 | −19.2 | ... |
| (A+B) | ... | 4.10 | ... | F5IV | ... | 3.06 | 35.776 | −58.2 | −26.1 | −31.18 |
| C | ... | 7.30 | 7.122 | G1V | 5705 | 1.00 | 35.822 | −75.0 | −12.0 | −30.35 |
| D | 144087 | 7.43 | 7.262 | G8V | 5622 | 0.97 | 35.911 | −61.6 | −22.2 | −31.58 |
| E | 144088 | 7.99 | 7.784 | K0V | 5330 | 0.91 | 35.844 | −56.4 | −20.3 | −31.96 |

TABLE 2
ORBITAL ELEMENTS

| System | $P$ yr | $T$ yr | $e$ | $a$ $''$ | $\Omega$ $^\circ$ | $\omega$ $^\circ$ | $i$ $^\circ$ | $\Sigma M$ $M_\odot$ | $K_1+K_2$ km s$^{-1}$ |
|---|---|---|---|---|---|---|---|---|---|
| I 27 C,D | 85.12 | 1916.92 | 0.039 | 1.094 | 141.0 | 135.7 | 31.3 | 1.67 | 4.2 |
| | ±0.11 | ±1.20 | ±0.002 | ±0.007 | ±0.9 | ±4.6 | ±0.5 | ±0.01 | ... |
| HJ 3423 A,B | 1200 | 2086.7 | 0.40 | 7.03 | 323.1 | 61.3 | 128.5 | 2.22 | 3.1 |
| | fixed | ±4.1 | fixed | ±0.07 | ±0.5 | ±1.6 | ±1.1 | ... | ... |
| STF 1998 A,B | 45.864 | 1997.215 | 0.7370 | 0.6666 | 23.86 | 165.61 | 34.37 | 3.06 | 10.1 |
| | ±0.046 | ±0.012 | ±0.0013 | ±0.0008 | ±0.49 | ±0.56 | ±0.31 | ±0.01 | ... |
| STF 1998 AB,C | 1514 | 2226 | 0.04 | 7.76 | 47.4 | 59.3 | 131.5 | 4.42 | 3.2 |

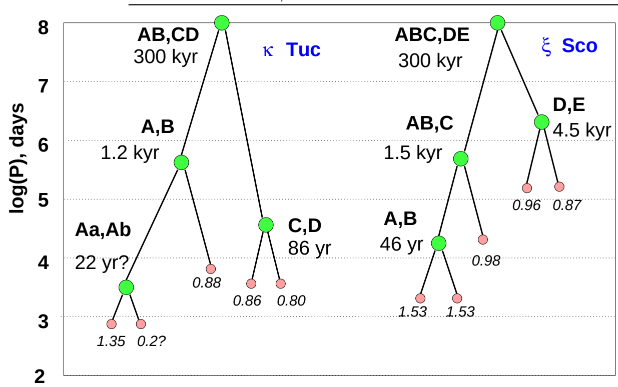


FIG. 1.— Architecture of $\kappa$ Tuc and $\xi$ Sco. The green circles represent subsystems, their vertical position corresponds to the logarithm of period in days, shown on the vertical axis. The small pink circles are individual stars, with their masses indicated below in italics.

of the center of mass are given in boldface. Astrometry comes from *Gaia*, radial velocities (RVs), effective temperatures and masses are discussed below. Figure 2 places the components on the Hertzsprung-Russell diagram (HRD) using data from Table 1 and compares with two solar-metallicity isochrones from Bressan et al. (2012). In both systems, massive components are slightly evolved.

I looked for potentially missed faint companions using *Gaia* and have not found any within projected distance of 50 kau from each system down to $M_G \sim 19$ mag, well below the end of the main sequence at $M_G \sim 11$ mag. This fact, together with the absence of detected spectroscopic subsystems, means that all stellar components are known.

## 2.2. *Motion of wide pairs*

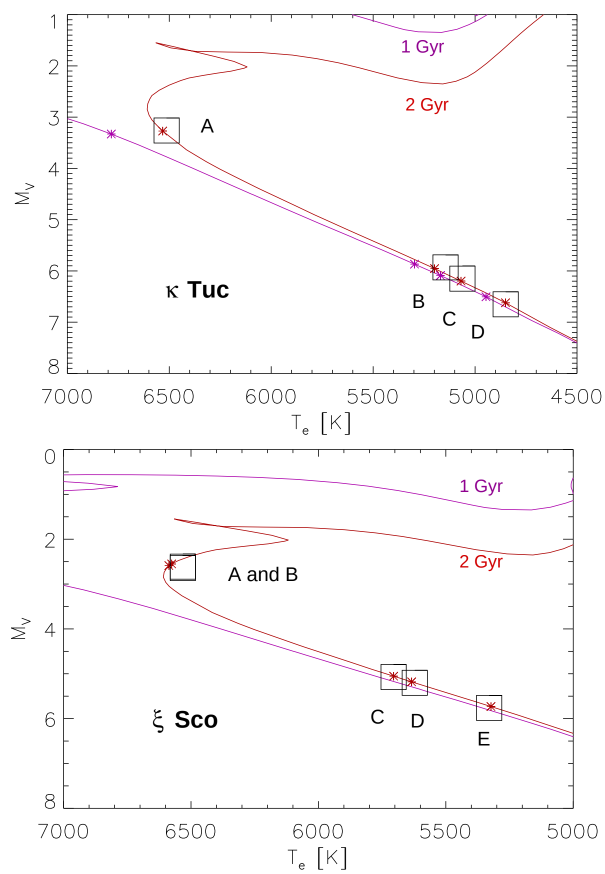


FIG. 2.— Hertzsprung-Russell diagram of $\kappa$ Tuc (top) and $\xi$ Sco (bottom) based on the data of Table 1. The magenta and red lines are PARSEC isochrones (Bressan et al. 2012) for solar metallicity and ages 1 and 2 Gyr, respectively. Asterisks on the isochrones mark the adopted masses of the components.

Precise parallaxes and PMs measured in the second *Gaia* data release (Gaia collaboration 2018) enable a new look at these wide hierarchies. However, knowledge of component's masses is needed to compute position and motion of the center of mass of the whole system or its constituents (subsystems). Good-quality visual orbits of subsystems, re-evaluated here, and precise parallaxes of all components provide mass measurements with a sub-percent accuracy. They agree with stellar isochrones (Figure 2), and therefore validate masses of other stars estimated from their absolute magnitudes using these isochrones.

Knowing PMs and masses, I compute the center of mass motion in the plane of the sky as mass-weighted *Gaia* PMs. Long periods are estimated from the third Kepler law by assuming that semimajor axis equals the projected separation $s$. These periods $P^*$ are valid in the statistical sense because the median of the $P^*$ distribution is close to the actual period $P$. The characteristic speed of the orbital motion $\mu^*$ is computed for a circular face-on orbit with a semimajor axis $s$ (Tokovinin & Kiyaeva 2017). The actual projected speed $\Delta\mu$ of a bound binary cannot exceed $\sqrt{2}\mu^*$. The normalized speed $\mu' = \Delta\mu/\mu^*$ is distributed in the range from zero to $\sqrt{2}$, with typical medians around 0.5. The angle $\gamma$ between relative motion in a wide pair and the radius-vector joining the components also contains some information on the orbit. The distribution of eccentricities can be inferred from the joint distribution of $\gamma$ and $\mu'$ (Tokovinin & Kiyaeva 2017). This cannot be done for individual systems, as is the case here, but the individual values of $\gamma$ and $\mu'$ still give some insight on the wide orbits.

RVs of the components bring additional information. They are essential to establish absence of inner subsystems and to check that the wide pair is bound, complementing $\mu'$. Unfortunately, the distance between components of a wide pair along the line of sight, $\Delta z$, is not known (the *Gaia* parallaxes are not accurate enough), otherwise a full orbit of a wide pair could be computed from its instantaneous position and relative velocity. Lacking this information, we may still compute a one-dimensional family of possible orbits and thus obtain some constraints. This is not done here because the difference of RVs between components or subsystems is not known with sufficient accuracy.

### 2.3. *Visual orbits*

Some inner subsystems have published visual orbits. I revise them here to compute accurate masses. The mass sum is proportional to $a^3/P^2$ ($a$ is the semimajor axis and $P$ is the period). These elements are usually positively correlated. Therefore, error of the mass sum estimated naively from the published errors of $a$ and $P$ would be too large. Moreover, weighting schemes adopted in fitting orbits by different authors lead to different solutions even if the data are the same. I use here weights inversely proportional to the square of measurement errors and assign large errors to the historic micrometer measurements, emphasizing instead accurate data from speckle interferometry and space missions. Orbital elements and their errors are determined using the IDL code `orbit.pro` (Tokovinin 2016b). The errors are checked by fitting many orbits with randomly perturbed data. This procedure also delivers realistic error of the ratio $a^3/P^2$, hence of the mass sum.

TABLE 3
CHIRON OBSERVATIONS

| Star | JD +24 00000 | RV km s$^{-1}$ | $A_{\rm CCF}$ | $\sigma_{\rm CCF}$ km s$^{-1}$ |
|---|---|---|---|---|
| $\kappa$ Tuc A | 57985.7954 | 8.042 | 0.036 | 31.15 |
| $\kappa$ Tuc B | 57985.7965 | 8.228 | 0.457 | 4.47 |
| $\xi$ Sco AB | 58922.7639 | −31.179 | 0.107 | 11.00 |
| $\xi$ Sco C | 58922.7672 | -30.350 | 0.470 | 3.63 |
| $\xi$ Sco D | 58920.8528 | −31.575 | 0.469 | 3.79 |
| $\xi$ Sco E | 58920.8564 | −31.961 | 0.514 | 3.88 |

Positional measurements used in the orbit fitting were retrieved from the Washington Double Star (WDS) Catalog database (Mason et al. 2001) and complemented by recent speckle data (Tokovinin et al. 2019) and relative positions measured by *Gaia*. Elements of the updated visual orbits and their errors are listed in Table 2. For completeness, the preliminary orbit of STF 1998 AB,C by Zirm (2008) is given in the last line. The penultimate column gives the mass sum computed from $a$, $P$, and adopted parallax. The errors of the mass sum do not account for errors of parallax (which are small for these nearby stars) and potential systematic errors that are difficult to evaluate. For stars with accurate orbits, the mass sums confirm mass estimates from the isochrones. Conversely, estimated masses help to constrain uncertain orbits computed from short arcs. The last column of Table 2 gives the full RV amplitudes computed from the orbital elements and masses.

### 2.4. *CHIRON spectroscopy*

High-resolution ($R \sim 80,000$) spectra were taken with the CHIRON optical echelle spectrometer (Tokovinin et al. 2013). The spectrograph is fiber-fed by the 1.5 m telescope located at the Cerro Tololo Interamerican Observatory (CTIO) and operated by Small & Moderate Aperture Research Telescope System (SMARTS) Consortium.[1] The data analysis is described in (Tokovinin 2016a). A cross-correlation function (CCF) of the reduced spectrum with a binary mask allows us to measure the RV. The amplitude $A_{\rm CCF}$ and dispersion $\sigma_{\rm CCF}$ of the Gaussian curve approximating the CCF dip contain information on the depth and width of spectral lines. The projected axial rotation $V \sin i$ is computed from $\sigma_{\rm CCF}$ using calibration in (Tokovinin 2016a). The results are given in Table 3. CHIRON spectra are discussed below jointly with other published spectroscopy.

## 3. $\kappa$ TUCANAE

$\kappa$ Tuc is composed of two resolved visual pairs. The brightest one A,B is $\kappa$ Tuc, HIP 5896, HD 7788, HR 377, GJ 55.3, and HJ 3423. Another pair C,D, at 318″ ($s$ = 6.7 kau) to the north-west from A,B, is known as HIP 5842, HD 7693, GJ 55.1, and I 27. This pair has a reliable visual orbit with a period of 85 yr (Soderhjelm 1999). Both pairs have common WDS code J01158−6853. Moreover, the brightest star A has an invisible astrometric companion detected by acceleration. The average parallax of other stars unaffected by acceleration (47.66 mas, distance 21.0 pc) is adopted. $\kappa$ Tuc

[1] http://www.astro.yale.edu/smarts/

belongs to the 25-pc sample of Raghavan et al. (2010), but they considered it quadruple because existence of the astrometric subsystem has not been established at the time.

### 3.1. *Visual orbits of $\kappa$ Tuc and subsystem Aa,Ab*

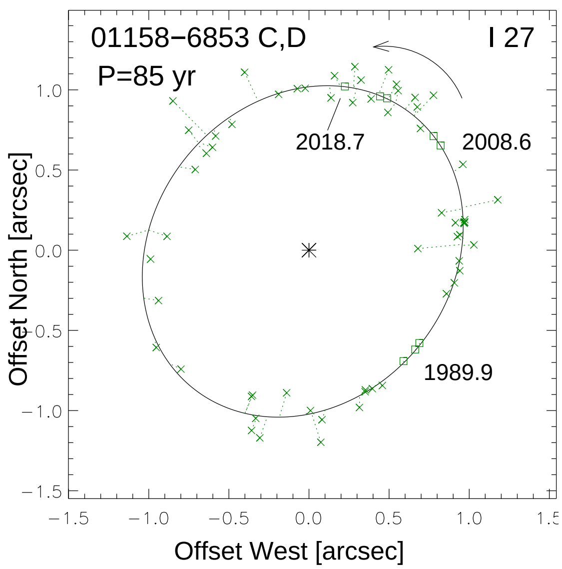


FIG. 3.— Orbit of $\kappa$ Tuc C,D (I 27). Accurate speckle measurements are plotted as squares, old micrometer measurements as crosses.

The orbit of C,D (I 27) by Soderhjelm (1999) has a grade 3 in the orbit catalog (Hartkopf et al. 2001). However, the orbit is accurately defined by the new data obtained after its calculation; 1.4 orbital periods are covered since the discovery of this pair (Figure 3). The corrected orbital elements of C,D and their errors are listed in Table 2. The mass sum is 1.67 $M_\odot$ for parallax of 47.66 mas. The relative uncertainly of the mass sum related to the orbit is $\Delta M/M = 0.006$. Note the small eccentricity and small inclination of the orbit to the plane of the sky, hence a nearly constant separation of $\sim$1″. The full RV amplitude $K_1 + K_2$ is only 4.2 km s$^{-1}$ owing to the small inclination and long period. Only a small RV variation of the blended spectrum of CD is expected; blending broadens the lines slightly, biasing the $V \sin i$ estimates.

J. Hershel discovered the pair $\kappa$ Tuc A,B in 1834.9 at 2″ and corrected his first discrepant measurement to 4.″75 in 1836. The orbit with $P = 857$ yr computed by Scardia & Pansechi (2005) is poorly constrained by the short observed arc (Figure 4). Adjustment of the orbit of A,B is needed for modeling its relative motion and searching for potential signature of the astrometric subsystem. I ignored a few most discrepant micrometer positions, assigned errors of 0.″5 to the rest, adopted errors of 30 mas for photographic positions available after 1947 and 5 mas for the *Gaia* relative position. The weighted residuals confirm the error model ($\chi^2/N \sim 1$). To avoid divergence and obtain the expected mass sum of 2.2 $M_\odot$, I had to fix the period and eccentricity. The new orbit of A,B (Figure 4) matches well accurate positions to the detriment of older micrometer data.

According to the adjusted orbit, in 2015.5 star B moved relative to A with a velocity of $(-10.72, -34.68)$

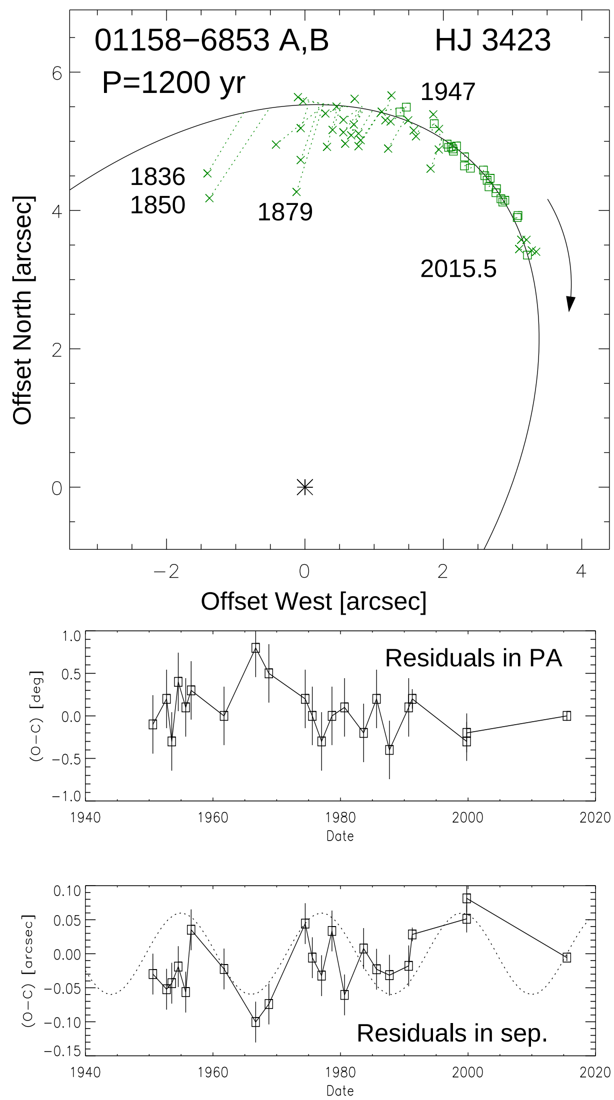


FIG. 4.— Orbit of $\kappa$ Tuc A,B (HJ 3423). Accurate photographic measurements are plotted as squares, micrometer measurements as crosses, component A is at the coordinate origin. The lower panel shows residuals of accurate measurements in angle and separation. The dotted line is a sine wave with a period of 22 yr and an amplitude of 60 mas.

mas yr$^{-1}$ in RA and Dec, respectively. Subtracting orbital motion from the PM of B, accurately determined by *Gaia*, I deduce the average PM of A as (397.0, 117.1) mas yr$^{-1}$. The average PM of A computed by Brandt (2018) from the difference between *Gaia* and *Hipparcos* positions is (396.6, 117.6) mas yr$^{-1}$. Good agreement between these almost independent PMs inspires confidence. The short-term PMs of A measured by both satellites are different from the average PM, and this *PM anomaly* $\Delta\mu$ is a reliable signature of the subsystem. Although *Gaia* astrometry of the bright star A is not very accurate (errors $\sim$1 mas), its PM anomaly is highly significant and independent of *Hipparcos*. According to Brandt (2018), $\Delta\mu_{HIP} = (14.9, 10.4)$ mas yr$^{-1}$ and $\Delta\mu_{Gaia} = (12.6, -10.6)$ mas yr$^{-1}$. During $\Delta T = 24.25$ yr elapsed between these space missions, the $\Delta\mu$ vector has turned by 75°(from 55° to 130°) with a roughly constant amplitude of 16 mas yr$^{-1}$.

Rotation of $\Delta\mu$ suggests a circular face-on orbit, and I adopt this as a starting hypothesis to guess orbital parameters of Aa,Ab. An anti-clockwise turn by 0.2 fraction of the full circle corresponds to the orbital period of $P = \Delta T/0.2 = 121$ yr. However, the subsystem could have made 0.8 revolutions clock-wise or 1.2 revolutions anti-clockwise during $\Delta T$ if the period is 30 or 20 yr, respectively. Residuals in separation in Figure 4 suggest a period $P = 22$ yr that I adopt as plausible. A sinusoidal signal with this period and an amplitude $\alpha = 60$ mas (dotted line) corresponds to the PM anomaly $\Delta\mu = 2\pi\alpha/P = 16$ mas yr$^{-1}$. The tentative sine curve shows an increasing separation in 2015.5, hence A moved to the south-east, in agreement with *Gaia* $\Delta\mu$. However, the residuals in angle do not show a signal with matching period and $0\overset{\circ}{.}7$ amplitude expected for a circular face-on orbit, therefore I refrain from fitting an astrometric orbit of the subsystem. Although the PM anomaly of star A is highly significant, the period of 22 yr is only a plausible guess, and other periods, e.g. $\sim$120 yr, cannot be ruled out.

A subsystem with $P = 22$ yr and a total mass of 1.55 $M_\odot$ has a semimajor axis of $0\overset{''}{.}43$ and the RV amplitude $(K_1 + K_2)/(\sin i) = 12$ km s$^{-1}$. The astrometric amplitude of 60 mas leads to the mass ratio $q = 0.16$ and $K_1/(\sin i) = 1.7$ km s$^{-1}$. A small inclination can easily explain the lack of detectable RV variation caused by the subsystem. A companion Ab of 0.2 $M_\odot$ implied by this period is too faint to be detectable in the spectrum or photometrically, but could be revealed by high-contrast imaging. If $P \approx 120$ yr, the companion needed to produce the observed PM anomaly should be more massive (0.4 $M_\odot$) and its semimajor axis would be $1\overset{''}{.}3$.

### 3.2. *Spectroscopy of κ Tuc*

Table 4 lists all available RV measurements of $\kappa$ Tuc. Nordström et al. (2004) measured two discordant RVs of A during 4 yr and concluded that its RV is variable with an amplitude of 17 km s$^{-1}$. This result prompted further observations with the aim of determining the spectroscopic orbit. Tokovinin et al. (2015) measured RVs of A, B, and CD with the echelle spectrograph at the 2.5 m Du Pont telescope. Later, Tokovinin (2015) used fiber echelle at the CTIO 1.5 m telescope and found the RV of A to be constant (rms scatter 0.28 km s$^{-1}$) from 10 spectra taken during 79 days. This excludes the short-period variability. Another spectrum taken at the same telescope with CHIRON in 2017 (Table 3) extents the time coverage to 7 yr with the same result, also confirmed by *Gaia* and Fuhrmann et al. (2017). The fast axial rotation of A ($V \sin i \approx 60$ km s$^{-1}$) prevents accurate measurement of its RV, but the data suggest that it changes slowly, if at all. The variability detected by Nordström et al. (2004) is likely caused by one wrong RV measurement. However, the data do not exclude a slow RV variability with an amplitude of $\sim$1 km s$^{-1}$ implied by the tentative orbit of Aa,Ab proposed above.

Effective temperature of A was measured at 6513 K by Ammler-von-Eiff & Reiners (2012), while Fuhrmann et al. (2017) found $T_e = 5145 \pm 90$ K for B. Ramírez et al. (2012) estimated $T_e = 5062 \pm 71$ K from the blended spectrum of CD and found these stars to be slightly metal-rich, [Fe/H]=0.14. The CD pair was monitored for exoplanets by Valenti et al. (2005), who give $T_e = 4982$ K and [M/H]=0.05. I adopt temperatures of 5062 and 4850 K for C and D, respectively. The CHIRON spectra of A and B show no trace of the lithium line and star B rotates slowly.

TABLE 4
Radial velocities of κ Tuc

| A | B | CD | Dates | Reference |
|---|---|---|---|---|
| 1.1? | ... | 6.1 | 1990-s | Nordström et al. (2004) |
| 7.4 | 8.3 | 5.6 | 2008 | Tokovinin et al. (2015) |
| 7.79 | ... | ... | 2010 | Tokovinin (2015) |
| 7.48 | 7.91 | ... | 2015.5 | Gaia collaboration (2018) |
| 9.4 | 8.25 | ... | 2015.9 | Fuhrmann et al. (2017) |
| 8.04 | 8.23 | ... | 2017.6 | CHIRON (this work) |

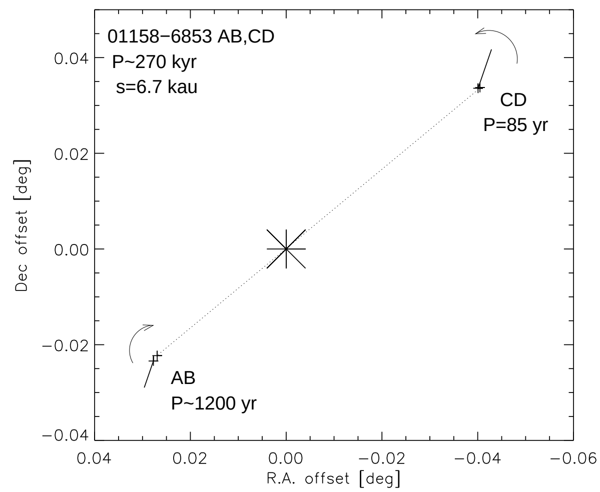


Fig. 5.— Position of four resolved components of $\kappa$ Tuc on the sky. Their motion relative to the center of mass (asterisk) is marked by short lines.

### 3.3. *Motion of κ Tuc AB,CD*

Proper motions of the centers of mass AB and CD are determined as mass-weighted *Gaia* PMs, with the exception of A, where *Gaia* PM is distorted by the subsystem. The PM of A is computed by subtracting the computed orbital motion of A,B from the measured PM of B, the mass of A, 1.55 $M_\odot$, accounts for the astrometric companion. Figure 5 shows the positions of four stars in the sky and the motions of the two pairs relative to the common center of mass.

CD moves relative to AB with the velocity $\Delta\mu = 2.89$ mas yr$^{-1}$ (0.29 km s$^{-1}$). The characteristic velocity is $\mu^* = 7.40$ mas yr$^{-1}$ (0.74 km s$^{-1}$), hence the normalized motion $\mu' = 0.39$, meaning that the system is bound. Relative motion is directed at an angle of 31° to the radius-vector, the separation between AB and CD increases. Note that the subsystems rotate in opposite sense (A,B clockwise and C,D anti-clockwise). The RV of CD is biased by the orbital motion, hence its difference with RVs of A and B is not significant.

### 3.4. *Age and kinematics of κ Tuc*

Figure 2 places components of $\kappa$ Tuc on the HRD. The masses of C and D derived from their absolute magnitudes and isochrone, 0.86 and 0.80 $M_\odot$, match the measured mass sum of CD, 1.67 $M_\odot$. The most massive star A is slightly evolved, suggesting an age of $\sim$2 Gyr. Estimates of the age found in the literature are inaccurate and discordant, but none indi-

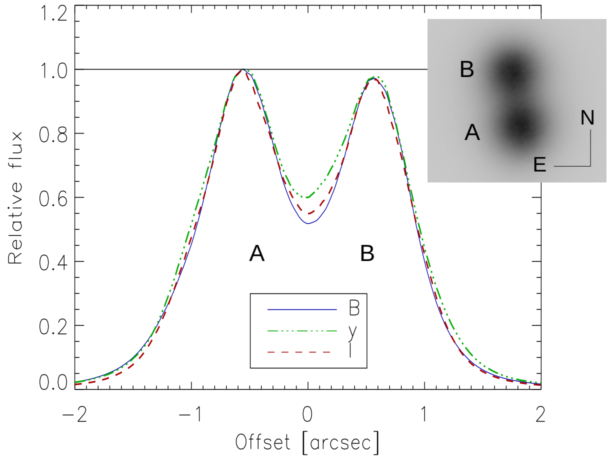


FIG. 6.— Scans of the re-centered average images of $\xi$ Sco AB taken on 2020-03-13 at SOAR in three filters. The flux is summed perpendicular to the binary, normalized by the maximum, and plotted along the separation direction. The northern component B is fainter than A by 3±1% in all filters. The insert shows the average image of this pair taken on 2017-06-06 in the filter $y$ (532 nm), separation 1.″127 and position angle 7.°8.

cates that these stars are young. The spatial motion $(U, V, W) = (-34.6, -21.5, -8.8)$ km s$^{-1}$ places this system among young disk population. Montes et al. (2001) noted similarity between motions of $\kappa$ Tuc and Hyades, $(U, W, U) = (-39.7, -17.7, -2.4)$. The multiple system might have originated in the same star-formation region, slightly enriched in metals relative to the Sun, but it is definitely older than the Hyades (otherwise the spectrum of B would contain the lithium line).

## 4. $\xi$ SCORPII

The system $\xi$ Sco contains five stars in a hierarchical configuration, recognized as such by van de Kamp & Harrington (1964). The main components A and B are known as HR 5978/5977, HD 144070/144069, WDS J16044−1122, STF 1998, and ADS 9909AB. Another star C is located at 7″ from AB. Further to the south, at an angular distance of 4.7′ (8 kau), there is a 12″ pair ADS 9910 (HIP 78738/78739, HD 144087/144088, STF 1999) with common PM, parallax, and RV (Table 1). Although ADS 9910 has a different WDS code 16044−1127, its components belong to the same system and are denoted here as D and E. Orbital motion in the 46-yr pair A,B was not included in the *Gaia* astrometric model, leading to inaccurate and oppositely biased parallaxes of A and B. However, their mean, 35.78 mas, matches perfectly the accurate (errors 0.05 mas) parallaxes of other stars. The average parallax of 35.84±0.03 mas is adopted in the following (distance 27.9 pc, distance modulus 2.23 mag).

### 4.1. *The pair $\xi$ Sco A,B (STF 1998)*

The components A and B, presently at 1.″1 separation, are so similar that there is some controversy about which of the two stars is brighter. The *Tycho* photometry indicates that B is brighter than A by 0.30 mag in both $V$ and $B$ bands, while the *Gaia* $G$ magnitudes of these stars are practically equal, but A appears to be slightly redder than B. However, *Gaia* low-resolution slitless spectroscopy might be seriously compromised by blending. It measured erroneous effective temperatures of A and B, 5096 and 5102 K, corresponding to spectral type K2. The combined $V - K$ color of AB, 1.21 mag, agrees with the actual spectral type F5IV. However, the infra-red photometry of AB in 2MASS is of poor quality because the image is heavily saturated.

The pair A,B is wide enough to be resolved in classical seeing-limited images, but no accurate published differential photometry was found. It was observed occasionally by the speckle camera at the Southern Astrophysical Research telescope (SOAR), but its photometry is usually biased by speckle anisoplanatism and image truncation in the standard 3″ field. Figure 6 shows an average re-centered image taken in 2017 in a wider 6″ field, without truncation. The experiment was repeated on 2020-03-13 in the filters $B$, $y$, and $I$. Scans through the images along the binary convincingly demonstrate that B is fainter than A by 3±1% in all three filters. Therefore, the colors of A and B are equal.

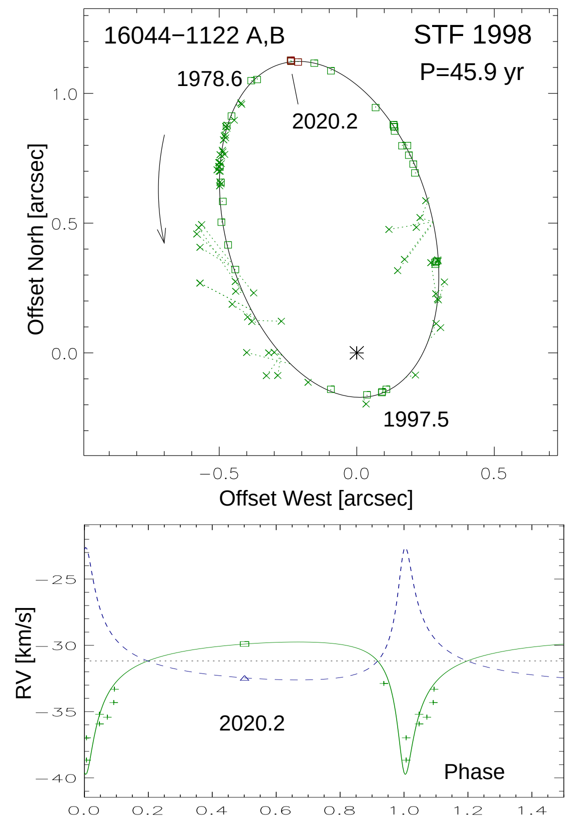


FIG. 7.— Orbit of STF 1998 A,B. Accurate speckle positions are plotted as squares (the latest ones in red), selected micrometer data as crosses. The lower plot shows the RV curve with amplitudes of 5 km s$^{-1}$. Crosses are RVs from Tokovinin & Smekhov (2002), square and triangle are the computed RVs in 2020.2.

The orbit of STF 1998 A,B is well defined (Docobo 2009). Speckle interferometry covers 41.6 yr, almost one full revolution. I re-fitted the orbit using only speckle data with appropriate weights and the *Gaia* relative position. Selected micrometer measurements around periastron passages in 1860 and 1905 are added with a low weight to better constrain the period. The adjusted orbit is shown in Figure 7, its elements are given in Table 2. The ratio $a^3/P^2$ is constrained with a relative error of 0.004. The parallax uncertainty contributes relative mass-sum error of 0.0025, the contribution of sys-

TABLE 5
Radial velocities of $\xi$ Sco

| AB | C | D | E | Reference |
|---|---|---|---|---|
| ... | ... | -31.80±0.30 | -32.30±0.20 | Nordström et al. (2004) |
| -36.3: | -30.90±0.27 | -31.82±0.29 | -32.67±0.36 | Tokovinin & Smekhov (2002) |
| ... | ... | -31.79±0.15 | -32.09±0.13 | Gaia collaboration (2018) |
| -31.18±0.1 | -30.3±0.05 | -31.58±0.05 | -31.96±0.05 | CHIRON (this work) |

tematic errors is uncertain but likely small. The mass sum of AB is known to better than a percent, 3.06±0.03 $M_\odot$. In 2020.2 B was located to the north of A at a separation of 1.″15, near the apastron. The last periastron passage happened in 1997.2.

van de Kamp & Harrington (1964) determined the fractional mass of B as 0.479 based on photographic astrometry of unresolved pair AB (motion of the photo-center relative to reference stars). As the stars A and B are very similar, the photocentric motion is small and its interpretation in terms of mass ratio depends on the adopted magnitude difference, which was quite uncertain at the time. The sign of the photocentric motion indicates that A is more massive than B.

The orbit predicts motion of B relative to A in 2015.5 with a velocity of $(+32.33, +15.42)$ mas yr$^{-1}$. The relative motion measured by *Gaia*, $(+32.40, +13.75)$ mas yr$^{-1}$, agrees rather well considering that these bright stars have less accurate astrometry and the *Gaia* linear astrometric solution does not account for the orbit. If the mean long-term PM of the pair AB were known, the mass ratio could be inferred from the individual PMs of A and B. The average PM of AB deduced from the *Gaia* PM of C and the uncertain orbit of AB,C does not differ significantly from the mean *Gaia* PM of A and B, indicating that the masses of A and B are approximately equal. Indeed, given the nearly equal fluxes and colors of A and B, the mass ratio in this pair must be very close to one.

The orbital elements and mass sum correspond to the total RV amplitude $K_1 + K_2 = 10.1$ km s$^{-1}$. Even at periastron, the pair is never spectrally resolved because the lines are broadened by rotation. The single-lined spectroscopic orbit by Chang (1929) with $K_1 = 3.7$ km s$^{-1}$ is very crude. The RVs of AB measured by Tokovinin & Smekhov (2002) around the 1997.2 periastron correspond to $K_1 = 2.9$ km s$^{-1}$ and $\gamma = -33.0$ km s$^{-1}$. The fact that the RV of the blended spectrum varies so much (60% of the expected full amplitude) implies that one of the components (presumably A) dominates in the blended spectrum, possibly because it rotates slower than the other and has sharper lines. The RV of the blended spectrum measured by CHIRON in 2020, $-31.18$ km s$^{-1}$, should be close to the center-of-mass RV. The CCF of AB is slightly asymmetric, but an attempt to model it by two Gaussians does not constrain their parameters well enough to be useful.

### 4.2. *Spectroscopy of $\xi$ Sco*

These bright stars has been repeatedly observed by spectroscopists for various reasons. They appear to be slightly metal-rich and chromospherically inactive (the weak X-ray radiation detected from DE is explained by its proximity to the Sun). AB is normally not resolved in seeing-limited spectroscopy, so its spectrum is a sum of two nearly equal stars. For AB, Ramírez et al. (2013) give $T_e = 6532$ K, $\log g = 4.16$, and [Fe/H]=0.02, while Casagrande et al. (2011) give $T_e = 6530 \pm 80$K and [Fe/H]=0.11. The catalog of Hinkel et al. (2017) gives for D and E, respectively, $T_e$ of 5542 and 5245 K, $\log g$ of 4.43 and 4.38, and [Fe/H] of 0.16 for both. For the same stars D and E, Nordström et al. (2004) estimated $T_e$ of 5420 and 5164 K and [Fe/H] of 0.06 and 0.09.

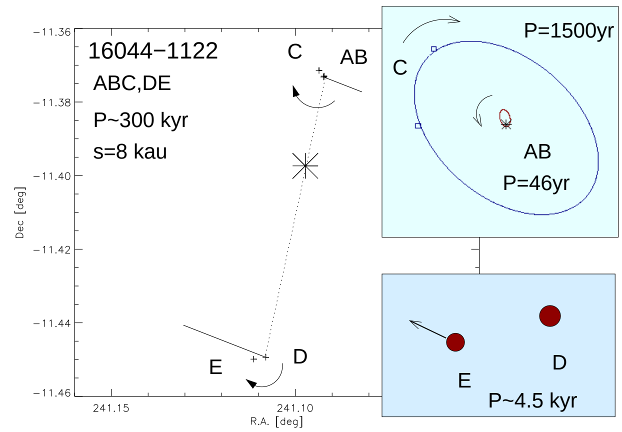


Fig. 8.— Location of $\xi$ Sco on the sky. The right-hand panels zoom on the two groups. The asterisk marks the center of mass, the lines show motion of group centers relative to it.

Spectra of the components AB, C, D, and E were taken with CHIRON in 2020 March. In the stars C, D, E the lines are narrow and correspond to $V \sin i$ of 2.3, 3.0, and 3.4 km s$^{-1}$, respectively. No lithium line or emissions are seen in those spectra. On the other hand, the CCF of AB is broad and corresponds to $V \sin i = 16.9$ km s$^{-1}$. In 2020, the RV difference between A and B was only 2.6 km s$^{-1}$, small compared to the rotationally-broadened lines. The lithium line 6708Å is present in the spectrum of AB with an equivalent width of 39±6 mÅ and a dispersion of 13.4 km s$^{-1}$.

The sharp-lined stars D and E have a constant RVs over a long time span (Table 5). The CHIRON spectra confirm the RV difference $\Delta V_{\rm ED} = -0.38$ km s$^{-1}$, matching previous measurements within 0.1 km s$^{-1}$. This constancy is a strong argument against existence of inner subsystems in D or E.

### 4.3. *Motion of $\xi$ Sco ABC,DE*

Figure 8 shows position of the stars on the sky and their relative motions determined as mass-weighted PMs. The PM of the center of mass of the whole system is $(-61.32, -22.19)$ mas yr$^{-1}$. The outermost pair ABC,DE rotates clockwise (retrograde). Its motion is almost perpendicular to the radius-vector joining ABC and DE and its speed is 3.52 mas yr$^{-1}$ (0.47 km s$^{-1}$). The projected separation $s = 8$ kau corresponds to $\mu^* = 6.20$ mas yr$^{-1}$ or 0.82 km s$^{-1}$, hence $\mu' = \Delta\mu/\mu^* = 0.57$. The outer system is definitely bound and its orbit likely has a moderate eccentricity because $\gamma \approx 90°$.

The intermediate pair AB,C has a preliminary (grade 5) visual orbit with $P = 1514$ yr (Zirm 2008). The upper-right panel shows this poorly constrained orbit determined from the observed 48° arc. This orbit corresponds to a plausible mass sum and a retrograde rotation. In contrast, A,B has a direct rotation and a large eccentricity.

The southern pair D,E has an estimated period of 4.5 kyr. The motion of E relative to D is retrograde, directed at an angle $\gamma \sim 30°$ relative to the radius-vector (E moves away from D). The speed of the relative motion in the D,E pair is 5.54 mas yr$^{-1}$ (0.73 km s$^{-1}$) and corresponds to $\mu' = 0.33$. Brandt (2018) found marginally significant astrometric accelerations of stars D and E from comparison between *Hipparcos* and *Gaia*. This implies existence of inner subsystems. However, *Hippacos* astrometry of double stars with separations of $10''$–$20''$ has known problems caused by its measurement system. This is the most likely explanation of spurious accelerations. Absence of subsystems follows from the constant RV difference between D and E.

### 4.4. *Age and kinematics of $\xi$ Sco*

Figure 2 uses effective temperatures (Table 1) to compare stellar parameters with the isochrones. For D and E, $T_e$ are estimated from the $V - K$ colors using the isochrone. For A and B, $T_e = 6532\,$K is adopted (Ramírez et al. 2013), while for C it corresponds to the spectral type G2V. The HRD shows that A and B have evolved off the main sequence, hence the system is about 2 Gyr old. The measured masses of A and B match the isochrone almost perfectly. In this region, the isochrone is vertical, explaining why A and B have the same color while differing slightly in luminosity. These stars are almost entirely radiative and have not fully depleted lithium in their atmospheres, while the less massive stars did.

The heliocentric spatial velocity of the system is $(U, V, W) = (-29.7, -7.5, -11.8)$ km s$^{-1}$ (U is directed away from the Galactic center). It does not match any known kinematic group. The age of $\sim$2 Gyr implies that the system $\xi$ Sco has been dynamically stable for a long time. Hence the two outer groups ABC and DE never come sufficiently close to each other to interact dynamically. This, in turn, means that the outer eccentricity is moderate. The motion direction in the outer orbit supports this view indirectly (a radial motion is expected in an eccentric orbit).

Anosova & Orlov (1991) studied dynamics of the triple subsystem ABC and concluded that it is unstable with a high probability. However, given the known orbit of AB,C and the system's age, dynamical instability is firmly excluded. These authors claim that the system belongs to a moving group that includes ADS 9910 and 12 other nearby stars listed in their Table 8. I retrieved modern data on those 12 stars from Simbad and computed their spatial motion. The mean velocity of the group (excluding the $\xi$ Sco system) is $(U, V, W) = (-30.8, -15.0, -12.8)$ km s$^{-1}$ and the rms scatter about the mean is $(4.1, 3.6, 3.7)$ km s$^{-1}$. The mean $V$ differs from the velocity of $\xi$ Sco by 7.5 km s$^{-1}$ ($2.1\sigma$), while the components $U$ and $W$ are similar. Spatial motions of stars in the Anosova's table, as well as of $\xi$ Sco, correspond to the young disk population, but modern data do not provide evidence of a putative kinematic group to which $\xi$ Sco might belong.

## 5. DISCUSSION

The quintuple systems $\kappa$ Tuc and $\xi$ Sco have several common properties: wide outer separations $s \sim 8$ kau, absence of tight spectroscopic subsystems, moderate age of $\sim$2 Gyr, and component's masses distributed in a narrow range between 0.8 and 1.5 $M_\odot$ (except the astrometric companion $\kappa$ Tuc Ab). The *Gaia* catalog indicates absence of additional low-mass companions at wide separations. In the hindsight, this is not surprising because low-mass stars with very wide separations would be torn apart during lifetime of these systems in the Galactic disk. At intermediate separations, there is little space in the hierarchy available for additional components (Figure 1). Although the dynamical stability criteria allow such subsystems to exist within certain ranges of separations, they could hardly escape detection either by *Gaia* direct resolution or by their astrometric signatures, as is the case of $\kappa$ Tuc Aa,Ab. Inner hierarchical levels remain free for close subsystems.

Distribution of masses in these systems presents a sharp contrast with moving groups and clusters which follow the standard initial mass function where low-mass stars dominate. Dynamical evolution in a cluster could lead to preferential binding of more massive stars in binaries while low-mass stars are ejected. However, wide outer separations of our hierarchies strongly speak against origin of these hierarchies in clusters. Dissolution of a cluster could leave behind wide bound pairs (Kouwenhoven et al. 2010), but it is unlikely that this process could create high-order hierarchies.

Our hierarchies also appear unusual from the binary-star perspective. Mass ratio of solar-type binaries is distributed almost uniformly independently of period (Raghavan et al. 2010; Tokovinin 2014). Here, all masses are similar, resembling in this sense low-mass binaries (Duchêne & Kraus 2013).

Most likely, these hierarchies formed by core fragmentation in a low-density environment, in relative isolation. As the gas density increases during collapse, the Jeans mass decreases, prompting further fragmentation that creates a hierarchical stellar system. At each fragmentation, a substantial part of the angular momentum of collapsing gas is retained in the orbital motion of the fragments around common center of mass, and this storage is most efficient when the fragment's masses are comparable. Therefore, a two-stage cascade fragmentation could produce a wide quadruple system of 2+2 hierarchy, i.e. two close pairs on a wide orbit around each other, with comparable masses. Such quadruple systems are indeed quite common, e.g. $\epsilon$ Lyr (see further discussion in Tokovinin 2008). The architecture of $\kappa$ Tuc matches this pattern, except the inner subsystem Aa,Ab.

However, in $\kappa$ Tuc the subsystems A,B and C,D rotate in the opposite sense, their orbits are definitely not coplanar. In $\xi$ Sco, the inner triple AB,C is misaligned. The angular momenta of the outer and inner subsystems obviously do not derive from a common source. A quick study of relative rotation sense in wide 2+2 quadruple systems found in the MSC confirms that rotation sense of their inner pairs is uncorrelated.

Masses of forming stars are not determined by the initial fragments, but, instead, are set by continuing accretion of gas for a relatively long time, compared to the free-fall time. This happens because small and dense regions collapse fast, while collapse at larger scale still continues. As a result, in a hierarchical collapse small-scale structures continue to accrete gas from larger scales (Vásquez-Semadeni et al. 2019). Components of a newly formed multiple system accrete from a common large-scale gas reservoir, producing stars with similar masses. Accretion also reduces the orbital separation (Lee et al. 2019; Tokovinin & Moe 2020).

Low-density star formation regions have a ubiquitous filamentary structure, with a typical filament width of 0.1 pc (20 kau). Gas from the surrounding cloud falls onto the filament roughly perpendicular to its axis, then changes direction and flows along the filament axis (Vásquez-Semadeni et al. 2019; Kuffmeier et al. 2019). Motions in a dense clump inside a filament are likely directed perpendicular to its axis, the angular momentum is hence roughly aligned with the filament axis, so fragmentation should produce a wide pair with an orbit perpendicular to the filament. However, the gas subsequently accreted by this system comes along the filament, so further fragmentation into subsystems and orientation of their orbits would be uncorrelated with the outer orbit or mutually. The accreted gas may contain additional fragments that fall onto the forming system, get captured by dynamical friction, and interact with other stars, as in the simulations by Lee et al. (2019), Kuffmeier et al. (2019), and Bate (2019).

The emerging formation scenario of $\kappa$ Tuc and $\xi$ Sco is a fragmentation of a relatively isolated clump in a low-density environment, its growth owing to prolonged accretion of gas flowing from large spatial scales (along the filament), further fragmentation into subsystems, and possible dynamical interactions with other fragments formed at a large distance. Comparable masses of components are explained by accretion from common gas reservoir. Misaligned orbits result from random gas motions and/or dynamical interactions. However, strong dynamical interactions between stars are ruled out because otherwise they would have destroyed the weakly bound outer pairs. Formation of wide binaries by dynamical ejection from unstable multiple systems, proposed by Reipurth & Mikkola (2012), does not match the architecture of these systems.

Stars do not form in isolation. Other members of the clouds that gave birth to our hierarchies were apparently unbound to them (too distant and with a too large relative velocity). A group of mutually unbound systems is seen as a YMG until it disperses. From this perspective, the fact than many YMGs contain high-order hierarchies appears natural. It still remains unclear why our two systems do not contain close pairs, unlike other more typical high-order hierarchies.

I thank the Referee, B. Mason, for pertinent comments. This work used the SIMBAD service operated by Centre des Données Stellaires (Strasbourg, France), bibliographic references from the Astrophysics Data System maintained by SAO/NASA, and the Washington Double Star Catalog maintained at USNO. This work has made use of data from the European Space Agency (ESA) mission *Gaia* (https://www.cosmos.esa.int/gaia), processed by the *Gaia* Data Processing and Analysis Consortium (DPAC, https://www.cosmos.esa.int/web/gaia/dpac/consortium). Funding for the DPAC has been provided by national institutions, in particular the institutions participating in the *Gaia* Multilateral Agreement.

*Facility:* CTIO:1.5m, SOAR

REFERENCES

Ammler-von-Eiff, M. & Reiners, A. 2012, A&A, 542, 116
Anosova, J. P. & Orlov, V. V. 1991, A&A, 252, 123
Bate, M. R. 2019, MNRAS, 484, 2341.
Brandt, T. D. 2018, ApJS, 239, 31
Bressan, A., Marigo, P., Girardi, L., et al. 2012, MNRAS, 427, 127
Caballero, J. A. 2010, A&A, 514, 98
Casagrande, L., Schörlich, R., Asplund, M. et al. 2011, A&A, 530, 138
Chang, Y. C. 1929, ApJ, 70, 182
Docobo, J. A. 2009, AJ, 138, 1159
Duchêne, G. & Kraus, A. 2013, ARAA, 51, 269 (ArXiv:1303:3028)
Fuhrmann, K., Chini, R., Kaderhardt, L., & Chen, Z. 2017, ApJ, 836, 139
Gaia Collaboration, Brown, A. G. A., Vallenari, A., Prusti, T. et al. 2018, A&A, 595A, 2 (Vizier Catalog I/345/gaia2).
Hartkopf, W. I., Mason, B. D., & Worley. C. E. 2001, AJ, 122, 3472
Hinkel, N. R., Mamajek, E. E., & Turnbull, M. C. 2017, ApJ, 848, 34
Kouwenhoven, M. B. N., Goodwin, S. P., Parker, R. P. et al. 2010, MNRAS, 404, 1835
Kuffmeier, M., Calcutt, H., & Kirstensen, L.. E. 2019, A&A, 628, 112
Lee, A. T., Offner, S., Kratter, K. et al. 2019, ApJ, 887, 232
Mason, B. D., Wycoff, G. L., Hartkopf, W. I., Douglass, G. G. & Worley, C. E. 2001, AJ, 122, 3466 (WDS)
Montes, D., Lopez-Santiago, J. Galvez, M. C. et al. 2001, MNRAS, 328, 45
Nordström, B., Mayor, M., Andersen, J. et al. 2004, A&A, 418, 989
Raghavan, D., McAlister, H. A., Henry, T. J. et al. 2010, ApJS, 190, 1
Ramírez, I., Fish, J. R., Lambert, D. L. & Allende-Prieto, C. 2012, ApJ, 756, 46
Ramírez, I., Allende Prieto, C. & Lambert, D. L. 2013, ApJ, 764, 78
Reipurth, B. & Mikkola, S. 2012, Nature, 492, 221
Scardia, M. & Pansecchi, L. 2005, Inf. Circ. 156, 1
Soderhjelm, S. 1999, A&A, 341, 121
Tokovinin A. A. & Smekhov M. G. 2002, A&A, 382, 118
Tokovinin, A. & Kiyaeva, O. 2017, MNRAS, 456, 2070
Tokovinin, A. 2008, MNRAS, 389, 925
Tokovinin, A., Fischer, D. A., Bonati, M. et al. 2013, PASP, 125, 1336
Tokovinin, A. 2014, AJ, 147, 87
Tokovinin, A., Pribulla, T., & Fischer, D. A. 2015, AJ, 149, 8
Tokovinin, A., 2015, AJ, 150, 177
Tokovinin, A. 2016a, AJ, 152, 11
Tokovinin, A. 2016cb ORBIT: IDL Software for Visual, Spectroscopic, and Combined Orbits, Zenodo, doi:10.2581/zenodo.61119
Tokovinin, A. 2018, ApJS, 235, 6
Tokovinin, A., Mason, B. D., Mendez, R. A. et al. 2019, AJ, 158, 48
Tokovinin, A. & Moe, M. 2020, MNRAS, 491, 5158
Valenti, J. A., Fischer, D. A. et al. 2005, ApJS, 159, 141
van de Kamp, P. & Harrington, R. S. 1964, AJ, 69, 402
Vásquez-Semadeni, E., Palau, A., Ballesteros-Paredes, J. et al. 2019, MNRAS, 490, 3061
Zirm, H. 2008, IAU Inf. Circ. 161, 1